

Clifford K. Ho

Sandia National Laboratories,
P.O. Box 5800, MS-1127,
Albuquerque, NM 87185-1127

Joshua M. Christian

Sandia National Laboratories,
P.O. Box 5800, MS-1127,
Albuquerque, NM 87185-1127

Julius E. Yellowhair

Sandia National Laboratories,
P.O. Box 5800, MS-1127,
Albuquerque, NM 87185-1127

Kenneth Armijo

Sandia National Laboratories,
P.O. Box 5800, MS-1127,
Albuquerque, NM 87185-1127

William J. Kolb

Sandia National Laboratories,
P.O. Box 5800, MS-1127,
Albuquerque, NM 87185-1127

Sheldon Jeter

Georgia Institute of Technology,
771 Ferst Drive,
Atlanta, GA 30332

Matthew Golob

Georgia Institute of Technology,
771 Ferst Drive,
Atlanta, GA 30332

Clayton Nguyen

Georgia Institute of Technology,
771 Ferst Drive,
Atlanta, GA 30332

On-Sun Performance Evaluation of Alternative High-Temperature Falling Particle Receiver Designs

This paper evaluates the on-sun performance of a 1 MW falling particle receiver. Two particle receiver designs were investigated: obstructed flow particle receiver versus free-falling particle receiver. The intent of the tests was to investigate the impact of particle mass flow rate, irradiance, and particle temperature on the particle temperature rise and thermal efficiency of the receiver for each design. Results indicate that the obstructed flow design increased the residence time of the particles in the concentrated flux, thereby increasing the particle temperature and thermal efficiency for a given mass flow rate. The obstructions, a staggered array of chevron-shaped mesh structures, also provided more stability to the falling particles, which were prone to instabilities caused by convective currents in the free-fall design. Challenges encountered during the tests included nonuniform mass flow rates, wind impacts, and oxidation/deterioration of the mesh structures. Alternative materials, designs, and methods are presented to overcome these challenges. [DOI: 10.1115/1.4041100]

1 Introduction

Conventional concentrating solar power systems that employ central receivers typically utilize a heat transfer fluid (e.g., water, molten salt, air, liquid metal) flowing through tubes or channels to cool the irradiated receiver. Falling particle receivers are being investigated to enable higher operating temperatures ($>700^\circ\text{C}$), inexpensive direct storage, and higher receiver efficiencies for concentrating solar power technologies and hydrogen production [1–16]. Unlike conventional receivers that employ fluid flowing through tubular receivers, falling particle receivers use solid particles that are heated directly as they fall through a beam of concentrated sunlight for direct heat absorption. Once heated, the particles may be stored in an insulated tank and used to heat a secondary working fluid for power generation or process heating. Previous studies have considered alternative particle receiver designs including free-falling [13,14], centrifugal [15,16], flow in tubes with or without fluidization [10,17,18], multipass recirculation [4,12], north- or south-facing [1,6], and face-down configurations [12].

In this paper, we present on-sun testing results of two particle receiver designs: (1) obstructed-flow particle receiver and (2) free-falling particle receiver. An overview of each design is presented along with the test procedure. The objectives of the test were to evaluate the effects of particle mass flow, irradiance, and particle temperature on the particle temperature rise and thermal efficiency of the receiver. Test results and challenges encountered during the tests are presented, along with methods to overcome the challenges.

2 System and Receiver Designs

Figure 1 shows the system and structure used to perform on-sun testing of the falling-particle receiver designs. The system consisted of $2\text{ m} \times 2\text{ m} \times 2\text{ m}$ cavity receiver with a $\sim 1\text{ m} \times 1\text{ m}$ aperture on the north side where concentrated sunlight entered the receiver. The ceramic particles (Accucast ID50; see Table 1¹) were released from a top hopper above the receiver and fell through the cavity (Fig. 2). Inside the cavity, the particles were irradiated by concentrated sunlight from a field of more than 200 heliostats at the National Solar Thermal Test Facility at Sandia National Laboratories. The south-facing polar heliostat field is

Contributed by the Solar Energy Division of ASME for publication in the JOURNAL OF SOLAR ENERGY ENGINEERING: INCLUDING WIND ENERGY AND BUILDING ENERGY CONSERVATION. Manuscript received January 29, 2018; final manuscript received July 23, 2018; published online September 14, 2018. Assoc. Editor: Marc Röger.

¹www.carboceramics.com

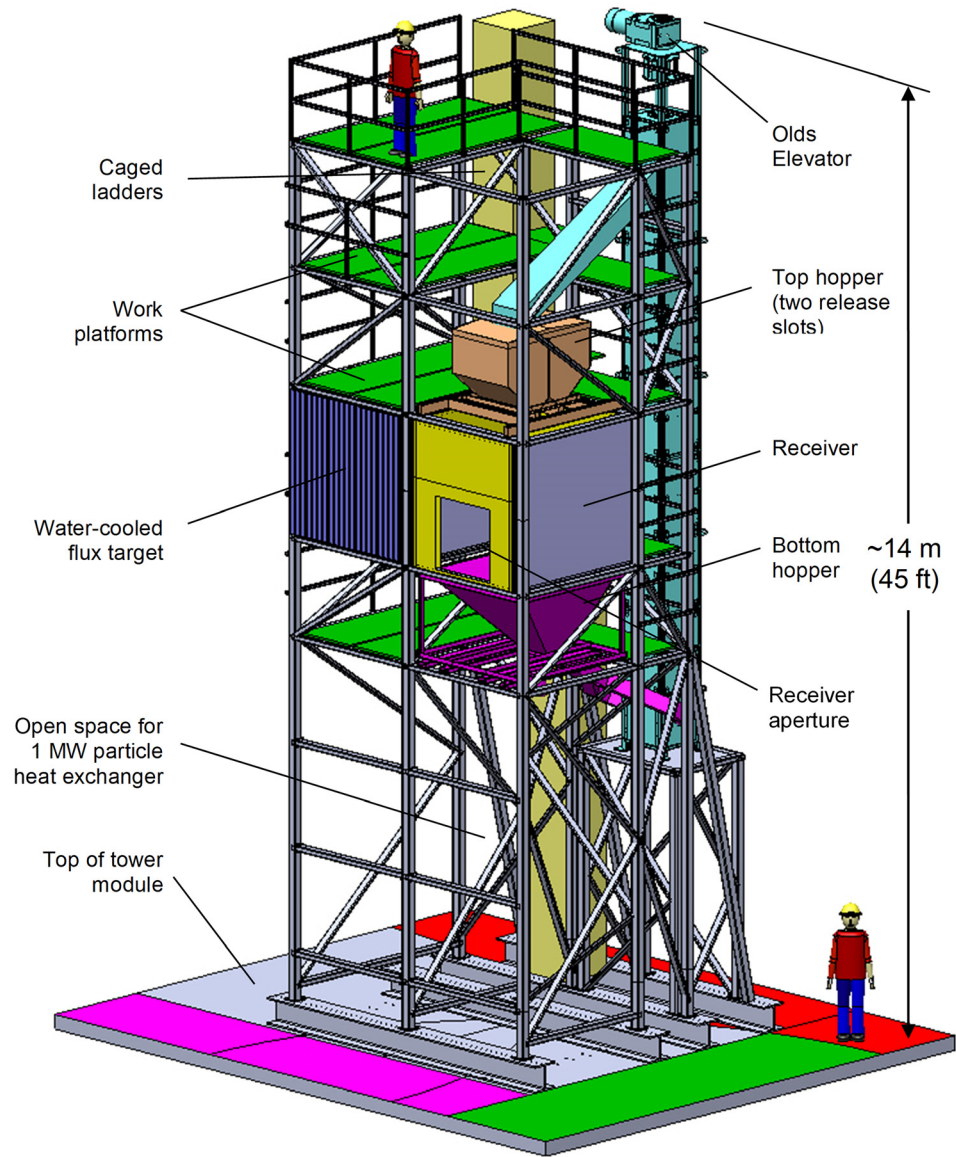


Fig. 1 Test structure for falling particle receiver system

Table 1 CARBO Accucast ID50 particle properties

Property	Value
Mass-median particle diameter (μm)	280
Particle density ^a (kg/m^3)	3300
Loose bulk density at 1100 °C (kg/m^3)	1810
Packed bed bulk density at 1100 °C (kg/m^3)	2000
Bulk porosity ^b	0.39 (packed) 0.45 (loose)
Packed bed bulk thermal conductivity at 1100 °C (W/m K)	0.7
Particle thermal conductivity ^c at 1100 °C (W/m K)	2
Specific heat ^d (J/kg K)	$365T^{0.18}$ for $50\text{ °C} \leq T \leq 1100\text{ °C}$
Packed-bed solar absorptance ^e	0.91
Packed bed thermal emittance ^f at 700 °C	0.75
Sphericity	0.9
Composition	75% Al_2O_3 , 11% SiO_2 , 9% Fe_2O_3 , 3% TiO_2

^aMeasured using Micromeritics AccuPyc 1330 pycnometer (courtesy Andrea Ambrosini, SNL)

^bCalculated from particle density and loose/packed bulk densities

^cCalculated using average of series and parallel bulk thermal conductivity models

^dFit to data from Netzsch STA 409 (courtesy Eric Coker, SNL)

^eMeasured as-received using Surface Optics 410-Solar. See Ref. [19] for degradation at elevated temperatures.

^fMeasured using Surface Optics ET-100 (courtesy James Yuan, SNL)

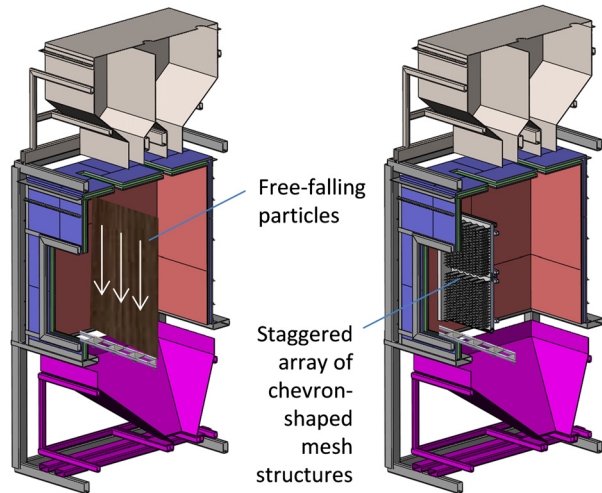


Fig. 2 Cutaway illustration of free-falling (left) and obstructed-flow (right) particle receiver designs

capable of generating up to 6 MW of thermal energy with 218 heliostats, each having 37 m^2 of reflective mirror area. After falling through the receiver, the particles were collected in a bottom hopper and funneled into a high temperature Olds particle elevator that lifted the particles inside a rotating casing surrounding a stationary auger. The particles were discharged into the top hopper, where the particles were released into the cavity receiver. The mass flow rate of particles falling into the receiver was controlled by a fixed slot aperture in a discharge plate at the base of the top hopper [20]. The receiver system was also included a water-cooled flux target with a Kendall radiometer that was used to measure and characterize the concentrated irradiance distribution from the heliostat field. The receiver system was instrumented with over 150 thermocouples to record temperatures throughout the system. At the base of the receiver, the particles flow through five funnels spaced evenly apart that allow the particles to accumulate and flow past a thermocouple immersed in the particles to measure the particle outlet temperature after being heated in the receiver (Fig. 2).

2.1 Obstructed-Flow Particle Receiver Design. The receiver design is shown in Fig. 2 and consisted of a staggered array of stainless-steel (SS316) chevron-shaped porous mesh structures ($\sim 0.6 \text{ mm}$ wire diameter with $\sim 2 \text{ mm}$ screen openings) affixed onto an insulating alumina board ($\sim 1.2 \text{ m}$ high \times 1.2 m wide; Fiberfrax Duraboard HD) placed inside of the cavity receiver under the front (north-most) discharge hopper [21]. The particles flowed through a discharge slot at the base of the top hopper and into the receiver (Fig. 2). The particle mass flow rate through the 1.24 m wide discharge slot (6.35 mm aperture) was measured to be 2.7 kg/s/m or 3.3 kg/s .² Inside the receiver, the particles flowed through and over the chevron-shaped mesh structures (similar to a Pachinko board) as they were irradiated by the concentrated solar flux entering through the aperture [22,23]. The width and depth of the chevrons was $\sim 7 \text{ cm} \times 13 \text{ cm}$, and the slot of the discharge plate was centered over the chevrons. The intent of the structures was to slow the particles and increase the residence time within the concentrated flux.

Figure 3 shows an image of the particles flowing through and around the chevron-shaped mesh structures. As described in Ho et al. [20,21], the mesh structures reduced the terminal velocity of the particles by nearly an order of magnitude from $\sim 5\text{--}6 \text{ m/s}$ to $\sim 0.5\text{--}0.8 \text{ m/s}$ at $1\text{--}2 \text{ m}$ of drop length. Although most of the

²The discharge plate was made of stainless steel 316 and expanded during heating. The slot aperture size changed, which also changed the particle mass flow rate as the system temperature increased as discussed in Sec. 4.3.1.

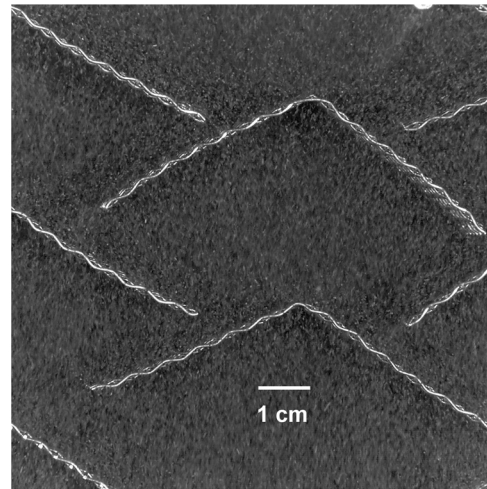


Fig. 3 Image showing particles flowing downward through and around chevron-shaped mesh structures

chevron surface was covered by flowing particles, the leading edge ($2\text{--}4 \text{ cm}$) was still visible and exposed to direct irradiance (Fig. 3). This led to oxidation and degradation of the mesh structures as described in Sec. 4.3.

2.2 Free-Fall Particle Receiver Design. In the free-fall particle receiver design, the panel containing the mesh structures for the obstructed-flow design was removed, and the particles flowed through one of two available discharge hoppers above the receiver (Fig. 2). A diverter valve was used to direct the particle flow to either of the hoppers, which were filled with particles. A discharge plate at the base of the hopper with a single slot opening distributed the particles uniformly along a straight line into the receiver. Alternate plates with different sized slot apertures were used to investigate the impact of different mass flow rates. Due to thermal expansion of the stainless-steel plates that were used in the obstructed-flow tests, which changed the particle mass flow rates as the temperatures increased (to $\sim 700^\circ \text{C}$), ceramic discharge plates were machined and used in the free-fall tests (see Sec. 4.3.1). Ho et al. [20] describe the characterization of the particle flow (velocity, opacity, curtain thickness, bulk density) as a function of the particle mass flow rate, which ranged from $\sim 3 \text{ kg/s}$ to 7 kg/s per meter of slot length.

3 Test Approach

A series of on-sun tests were performed to evaluate the two receiver designs with the continuously recirculating falling particle receiver system at the National Solar Thermal Test Facility at Sandia National Laboratories. The obstructed flow tests were conducted in June and July 2015, and the free-fall tests were conducted from September through November 2015. In each test, heliostats were selected to provide a desired irradiance on the receiver. The irradiance distribution on the receiver was characterized by using photographic images of the combined heliostat beams on the water-cooled flux target adjacent to the receiver (Fig. 1). The irradiance on the flux target was photographed, and a Kendall radiometer located in the center of the flux target provided an irradiance measurement that was used to scale the pixel values. The ray-tracing tool SolTrace was used to identify heliostat configurations that would produce a desired peak flux and power into the receiver. The residence time of the particles in the concentrated beam of light was approximately $0.2\text{--}0.4 \text{ s}$ for the free-falling design and $1\text{--}3 \text{ s}$ for the obstructed flow design based on measured velocities and the height of the illuminated region. Particle velocities were measured during off-sun tests using



Fig. 4 Images of on-sun testing of the particle receiver at the national solar thermal test facility

particle image velocimetry, and terminal velocities were found to be $\sim 0.5\text{--}0.8$ m/s [24].

Thermocouples were used to measure the particle temperatures at several locations at the inlet and outlet of the receiver. The power absorbed by the particles was determined by the particle mass flow rate, specific heat, and inlet and outlet temperatures. The thermal efficiency was determined as the ratio of the absorbed power to the incident power

$$\eta_{\text{th}} = \frac{Q_{\text{abs}}}{Q_{\text{in}}} = \frac{\dot{m}(h_{\text{out}} - h_{\text{in}})}{Q_{\text{in}}} = \frac{\dot{m} \int_{T_{\text{in}}}^{T_{\text{out}}} c_p(T) dT}{Q_{\text{in}}} = \frac{\dot{m} \left[\frac{365}{1.18} (T_{\text{out}}^{1.18} - T_{\text{in}}^{1.18}) \right]}{Q_{\text{in}}} \quad (1)$$

where Q_{abs} is the power absorbed by the particles (W), h is the enthalpy of the particles (J/kg), \dot{m} is the particle mass flow rate, Q_{in} is the incident power on the particles, and T_{in} and T_{out} are the inlet and outlet particle temperatures, respectively. In Eq. (1), the following relation [20] derived from measured data for the particle specific heat as a function of temperature (in degrees Celsius) was used

$$c_p(T) = 365T^{0.18} \quad (2)$$

The following protocol was implemented during the tests: (1) turn on the particle elevator to begin particle flow through the system; (2) aim the prescribed heliostats at the water-cooled flux target and measure the irradiance; (3) aim the heliostats at the receiver aperture and heat the particles to a desired (bulk) temperature entering the receiver; (4) at the desired temperature, remove the heliostats and allow the particles to mix and temperatures to stabilize; (5) aim the prescribed heliostats at the receiver aperture to heat the particles and allow temperatures to stabilize for several minutes; (6) aim heliostats at water-cooled flux target and measure irradiance; (7) repeat steps (3)–(6) as necessary to evaluate particle temperature rise and thermal efficiency at different temperatures. Figure 4 shows images of the particle receiver testing.

4 Test Results

4.1 Obstructed-Flow Results. Figures 5 and 6 shows the increase in particle temperature per unit drop length and the thermal efficiency, respectively, as a function of the average irradiance on the aperture for the obstructed-flow particle receiver tests (the average irradiance on the particles was simulated to be $\sim 80\%$ of the average irradiance on the aperture). The values were recorded for average particle temperatures of $\sim 440\text{--}660$ °C. Results show that the average particle temperature rise ranged

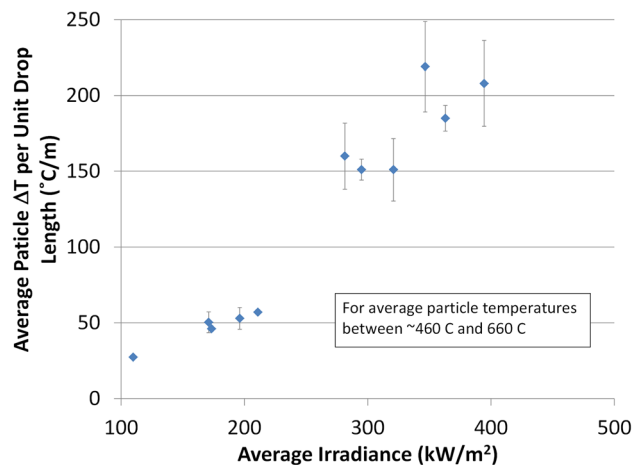


Fig. 5 Measured increase in particle temperature versus average irradiance for the obstructed-flow receiver design. Error bars represent one standard deviation.

from ~ 50 °C/m for average irradiances of ~ 200 kW/m² to $150\text{--}200$ °C/m for average irradiances of $300\text{--}400$ kW/m². The thermal efficiency (Eq. (1)) ranged from 0.5 to 0.6 for the lower irradiances to above 0.8 for the higher irradiances. The average particle temperature between the inlet and outlet of the receiver

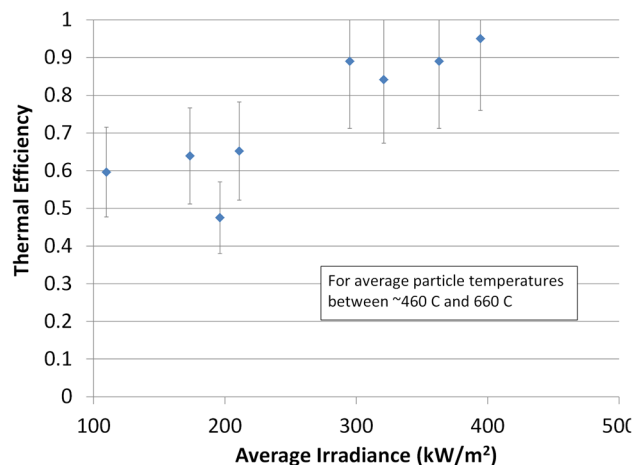


Fig. 6 Measured thermal efficiency versus average irradiance for the obstructed-flow receiver design. Error bars represent one standard deviation.

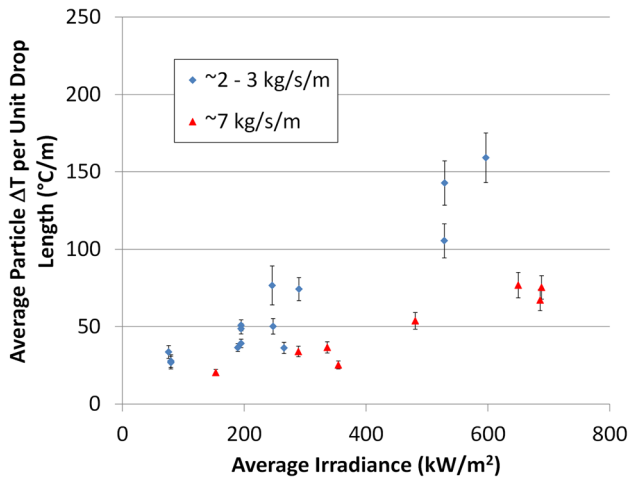


Fig. 7 Measured increase in particle temperature versus average irradiance for the free-fall receiver design. Error bars represent one standard deviation.

was between 440 °C and 660 °C, with bulk outlet temperatures exceeding 700 °C for several of the tests.

Challenges encountered during the obstructed-flow tests included thermal expansion of the stainless steel discharge plates, which reduced the slot aperture and particle mass flow rate near the center of the slot. This was determined by measuring the slot aperture after the tests and measuring the discharge time for the particle inventory to determine the reduced mass flow rate (from ~3 kg/s to less than 2 kg/s). As a result, the mesh structures overheated in the center, where the highest flux was located, and deteriorated (see Sec. 4.3.2). Only one discharge plate (6.35 mm aperture) was used during the tests before the mesh structures deteriorated.

4.2 Free-Fall Results. Figures 7 and 8 show the increase in particle temperature per unit drop length and the thermal efficiency, respectively, as a function of the average irradiance on the aperture for the free-fall particle receiver tests. In these tests, different slot apertures were used to produce different particle mass flow rates. In the plots, the results are categorized between low-flow (~2–3 kg/s/m) and high-flow (~7 kg/s/m) conditions. The mass flow is reported per unit length of the slot to normalize tests where the slot lengths were different. In the high-flow cases, the slot had to be reduced to accommodate the limited particle mass flow through the diverter valve and discharge chute (~4 kg/s).

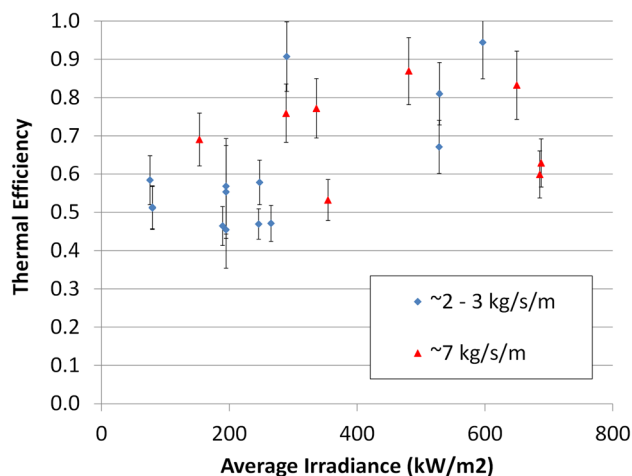


Fig. 8 Measured thermal efficiency versus average irradiance for the free-fall receiver design. Error bars represent one standard deviation.

Results show that the average particle temperature rise ranged from ~30 to 50 °C/m for average irradiances of ~200 kW/m² to 100 to 150 °C/m for average irradiances of ~600 kW/m² at low flow rates. At the higher particle flow rate, the average particle temperature rise was less due to the increased thickness and opacity of the particle curtain, which created additional shading. The thermal efficiency ranged from 0.4 to 0.6 for the lower irradiances at the lower flow rate; at the higher flow rate, the efficiency increased to 0.7–0.8. At higher irradiances (~600 kW/m²), the thermal efficiency was quite scattered and ranged from 0.6 to 0.9 for both the low and high mass flow rates. At these higher irradiances, it became more difficult to get representative particle outlet temperatures due to additional convection that affected the readings and particle flow into the thermocouple funnels.

The average particle temperature ranged from ~100 °C to 600 °C during the tests. In general, the average particle temperature did not show a strong correlation to the particle temperature increase or the thermal efficiency, although the measurements at higher particle temperature generally were associated with higher irradiances.

The particle temperature rise per unit drop length was greater for the obstructed-flow design due to the increased residence time of the particles in the concentrated sunlight. The thermal efficiency of the obstructed-flow design was generally higher as well for the irradiances tested. The slow particle velocities in the obstructed-flow design reduced convective heat losses and flow instabilities of the particles observed in the free-fall tests. In addition, the opacity of the falling particles was increased, which reduced light transmittance and potential for reflective losses.

4.3 Challenges and Discussion

4.3.1 Nonuniform Mass Flow Rates. The slotted particle discharge plates initially used in the on-sun tests were made of stainless steel 316. During on-sun testing, these plates increased in temperature (to over ~600 °C) as the heated particles flowed over the plate. During the tests, the particle mass flow rate appeared to be reduced near the center of the discharge slot as evidenced by greater light transmittance through the curtain. After removing the plates from the top hopper, the slot aperture was measured with digital calipers along the length of the slot and is plotted in Fig. 9 for two different plates used in the front and back hoppers. The apertures near the center of slot had reduced by over 30% from ~6 mm to ~4 mm after exposure to temperatures over 500 °C.

A finite element model of the heated discharge plate was developed to evaluate the cause of the aperture reduction. Results showed that if the outside edges of the plate were constrained

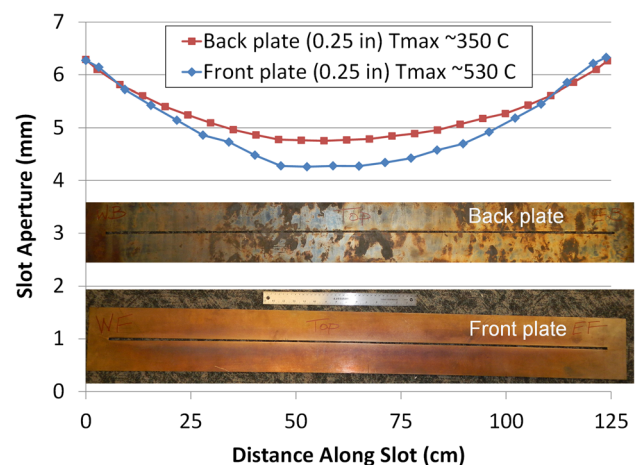


Fig. 9 Measured slot aperture after on-sun testing and heating for two different plates (both initially 6.35 mm aperture) heated to different temperatures

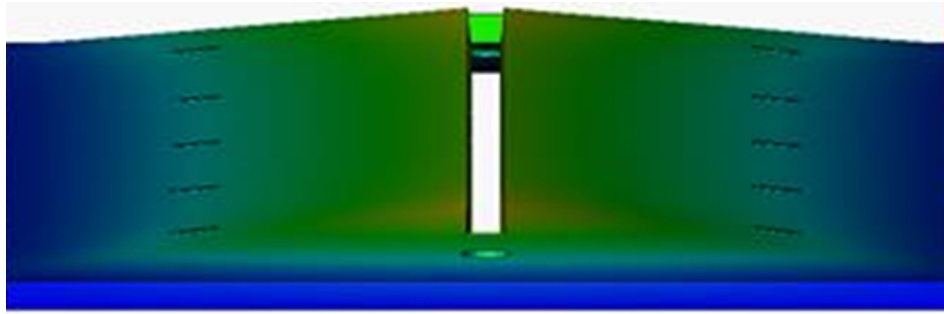


Fig. 10 Finite element simulation of heated stainless steel 316 discharge plate (700 °C) confined along the bottom edges, resulting in buckling and narrowing of the aperture

(due to particles surrounding the plate), the plate would buckle upward and the aperture would shrink (see Fig. 10).

Tests were performed to further evaluate the aperture changes in the discharge plates as a function of temperature. Figure 11 shows the measured aperture size as a function of distance along the slot during heater tests. The plate was wrapped in resistive heating wire, wrapped in insulation, and heated to 500 °C and 700 °C. The aperture was then measured as a function of distance along the plate while it was still hot. Although the plate was unconstrained, the results still showed that the aperture decreased in size, with a greater reduction at higher temperatures. Unlike the heated plates that were constrained by the particles, the unconstrained plate showed a greater reduction in aperture near the edges rather than at the center, possibly indicating some twisting or warping.

To mitigate the effects of heating on reduced aperture size and particle mass flow rate, discharge plates were fabricated from silica (RSLE-57). These plates were used in most of the free-fall tests and were shown to maintain a nearly constant aperture, even at high temperatures, based on the top-hopper discharge times during on-sun tests.

4.3.2 Deterioration of Mesh Structures. After ~20h of on-sun testing at irradiance up to ~700 kW/m², the mesh structures used in the obstructed-flow tests failed (see Fig. 12). SEM and EDS analysis of the deteriorated mesh structures revealed that

severe oxidation of the stainless steel wire occurred. A chrome oxide shell formed that was abraded by the falling particles, causing the mesh to become very brittle. Evidence of the stainless steel melting was observed, indicating that temperatures had exceeded ~1400 °C (melting point of SS316). The particles had sintered onto the oxide, but did not show signs of melting, indicating that the temperature remained less than ~2000 °C (Fig. 12). Previous testing has shown that the ceramic particles used in these tests (CARBO Accucast ID-50) are very durable and did not show significant signs of wear or sintering after thousands of drop cycles in a rotating vessel heated to 1000 °C [25]. Evaluation of the wear (size reduction) and radiative properties of the particles used in

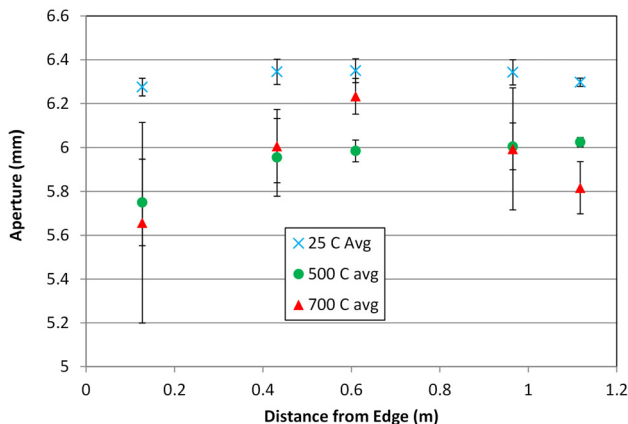


Fig. 11 Change in aperture during tests of stainless-steel 316 discharge plate with initial 6.35 mm slot aperture

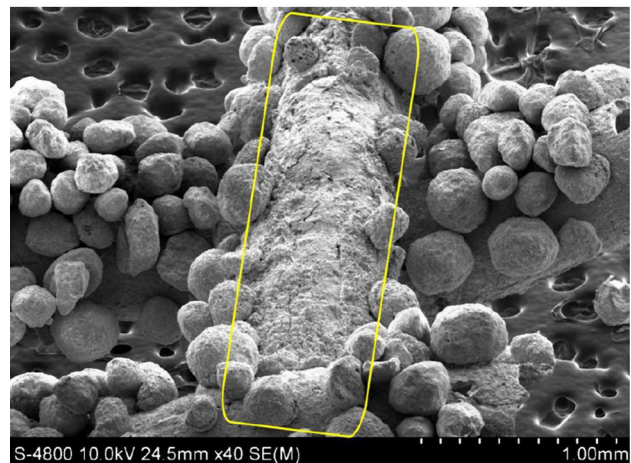


Fig. 12 Deteriorated mesh structure (top) and SEM image of oxidized wire mesh with sintered particles

the current study will be detailed in a future paper after testing is completed.

The high temperatures and failure of the mesh were caused, in part, by the reduced particle mass flow rate through the slot aperture, which shrunk with heating, causing the mesh to overheat. Future obstructed-flow tests will use ceramic discharge plates to maintain a consistent particle mass flow and cooling. Alternative materials for the mesh structures are also being evaluated, including Inconel 600, Inconel 601, Monel 400, Incoloy 800, Hasteloy C276, Hasteloy X, Kanthal D, titanium alloy, and ceramics.

5 Conclusions

Two high-temperature particle receiver designs have been developed and tested. The impact of irradiance, particle mass flow rate, and particle temperature on the particle temperature rise and thermal efficiency were investigated. Results showed that the obstructed-flow particle receiver design yielded greater increases in particle temperature relative to the free-fall particle receiver. The particle temperature increase was $\sim 200^\circ\text{C}/\text{m}$ for average irradiances up to $\sim 400\text{ kW}/\text{m}^2$ for the obstructed-flow tests. The particle temperature increase for the free-fall tests was $100\text{--}150^\circ\text{C}/\text{m}$ for irradiances up to $\sim 600\text{ kW}/\text{m}^2$. The particle temperature rise was correlated to the particle mass flow rate in the free-fall tests. Higher mass flow rates yielded lower particle temperature increases due to a thicker and more opaque curtain that cause more particle shading. However, the thermal efficiency was generally increased with higher mass flow rates due to the greater absorption of the irradiation.

The thermal efficiency was also higher for the obstructed-flow design. Efficiencies ranged from ~ 50 to 90% , with higher thermal efficiencies corresponding to higher irradiances up to $\sim 400\text{ kW}/\text{m}^2$. The free-fall tests yielded thermal efficiencies between ~ 50 and 80% with irradiances up to $\sim 400\text{ kW}/\text{m}^2$.

Technical challenges that were encountered during the tests included nonuniform and variable mass flow rates and deterioration of the mesh structures. During on-sun testing, the plates expanded and warped, causing the slot to narrow in the middle. This caused the mass flow of particles in the center of the receiver to decrease, which caused the mesh materials to overheat, oxidize, and deteriorate. Alternative materials and designs have been investigated for both the discharge plate and mesh materials to reduce thermal expansion, wear, and oxidation.

Acknowledgment

The authors thank JJ Kelton, Daniel Ray, Kye Chisman, Doug Robb, Benson Tso, Ryan Anderson, Ron Briggs, and Steve Hinken for their contributions to the receiver assembly and testing. This work was funded by the DOE SunShot program. This paper describes objective technical results and analysis. Any subjective views or opinions that might be expressed in the paper do not necessarily represent the views of the U.S. Department of Energy or the United States Government. Sandia National Laboratories is a multimission laboratory managed and operated by National Technology and Engineering Solutions of Sandia, LLC, a wholly owned subsidiary of Honeywell International, Inc., for the U.S. Department of Energy's National Nuclear Security Administration under contract DE-NA0003525.

Funding Data

- Solar Energy Technologies Program (SunShot 1558).

References

- [1] Christian, J. M., and Ho, C. K., 2014, "Alternative Designs of a High Efficiency, North-Facing, Solid Particle Receiver," *Energy Procedia*, **49**, pp. 314–323.
- [2] Falcone, P. K., Noring, J. E., and Hruby, J. M., 1985, "Assessment of a Solid Particle Receiver for a High Temperature Solar Central Receiver System," Sandia National Laboratories, Livermore, CA, Report No. SAND85-8208.
- [3] Gobereit, B., Amsbeck, L., Buck, R., Pitz-Paal, R., and Müller-Steinhagen, H., 2015, "Assessment of a Falling Solid Particle Receiver With Numerical Simulation," *Solar Energy*, **115**, pp. 505–517.
- [4] Ho, C., Christian, J., Gill, D., Moya, A., Jeter, S., Abdel-Khalik, S., Sadowski, D., Siegel, N., Al-Ansary, H., Amsbeck, L., Gobereit, B., and Buck, R., 2014, "Technology Advancements for Next Generation Falling Particle Receivers," *Solarpaces 2013 International Conference*, pp. 398–407.
- [5] Hruby, J. M., and Steele, B. R., 1986, "A Solid Particle Central Receiver for Solar-Energy," *Chem. Eng. Prog.*, **82**(2), pp. 44–47.
- [6] Khalsa, S. S. S., Christian, J. M., Kolb, G. J., Röger, M., Amsbeck, L., Ho, C. K., Siegel, N. P., and Moya, A. C., 2011, "CFD Simulation and Performance Analysis of Alternative Designs for High-Temperature Solid Particle Receivers," *ASME Paper No. ES2011-54430*.
- [7] Khalsa, S. S. S., and Ho, C. K., 2011, "Radiation Boundary Conditions for Computational Fluid Dynamics Models of High-Temperature Cavity Receivers," *ASME J. Sol. Energy Eng.*, **133**(3), p. 031020.
- [8] Kim, K., Moujaes, S. F., and Kolb, G. J., 2010, "Experimental and Simulation Study on Wind Affecting Particle Flow in a Solar Receiver," *Sol. Energy*, **84**(2), pp. 263–270.
- [9] Kolb, G. J., Diver, R. B., and Siegel, N., 2007, "Central-Station Solar Hydrogen Power Plant," *ASME J. Sol. Energy Eng.*, **129**(2), pp. 179–183.
- [10] Ma, Z. W., Glatzmaier, G., and Mehos, M., 2014, "Fluidized Bed Technology for Concentrating Solar Power With Thermal Energy Storage," *ASME J. Sol. Energy Eng.*, **136**(3), p. 031014.
- [11] Rightley, M. J., Matthews, L. K., and Mulholland, G. P., 1992, "Experimental Characterization of the Heat-Transfer in a Free-Falling-Particle Receiver," *Sol. Energy*, **48**(6), pp. 363–374.
- [12] Röger, M., Amsbeck, L., Gobereit, B., and Buck, R., 2011, "Face-Down Solid Particle Receiver Using Recirculation," *ASME J. Sol. Energy Eng.*, p. 031009.
- [13] Siegel, N. P., Ho, C. K., Khalsa, S. S., and Kolb, G. J., 2010, "Development and Evaluation of a Prototype Solid Particle Receiver: On-Sun Testing and Model Validation," *ASME J. Sol. Energy Eng.*, **132**(2), p. 021008.
- [14] Tan, T. D., and Chen, Y. T., 2010, "Review of Study on Solid Particle Solar Receivers," *Renewable Sustainable Energy Rev.*, **14**(1), pp. 265–276.
- [15] Wu, W., Trebing, D., Amsbeck, L., Buck, R., and Pitz-Paal, R., 2015, "Prototype Testing of a Centrifugal Particle Receiver for High-Temperature Concentrating Solar Applications," *ASME J. Sol. Energy Eng.*, **137**(4), p. 041011.
- [16] Wu, W., Uhlig, R., Buck, R., and Pitz-Paal, R., 2015, "Numerical Simulation of a Centrifugal Particle Receiver for High-Temperature Concentrating Solar Applications," *Numer. Heat Transfer Part A-Appl.*, **68**(2), pp. 133–149.
- [17] Flamant, G., Gauthier, D., Benoit, H., Sans, J. L., Boissiere, B., Ansart, R., and Hemati, M., 2014, "A New Heat Transfer Fluid for Concentrating Solar Systems: Particle Flow in Tubes," *Solarpaces 2013 International Conference*, pp. 617–626.
- [18] Flamant, G., Gauthier, D., Benoit, H., Sans, J. L., Garcia, R., Boissiere, B., Ansart, R., and Hemati, M., 2013, "Dense Suspension of Solid Particles as a New Heat Transfer Fluid for Concentrated Solar Thermal Plants: On-Sun Proof of Concept," *Chem. Eng. Sci.*, **102**, pp. 567–576.
- [19] Siegel, N., Gross, M., Ho, C., Phan, T., and Yuan, J., 2014, "Physical Properties of Solid Particle Thermal Energy Storage Media for Concentrating Solar Power Applications," *Solarpaces 2013 International Conference*, pp. 1015–1023.
- [20] Ho, C. K., Christian, J. M., Romano, D., Yellowhair, J., and Siegel, N., 2015, "Characterization of Particle Flow in a Free-Falling Solar Particle Receiver," *ASME Paper No. ES2015-49421*.
- [21] Ho, C. K., Christian, J. M., Yellowhair, J., Siegel, N., Jeter, S., Golob, M., Abdel-Khalik, S. I., Nguyen, C., and Al-Ansary, H., 2015, "On Sun Testing of an Advanced Falling Particle Receiver System," *AIP Conf. Proc.*, **1734**, p. 030022.
- [22] Khayyat, A. W., Knott, R. C., Nguyen, C. L., Golob, M. C., Abdel-Khalik, S. I., Jeter, S. M., and Al-Ansary, H. A., 2015, "Measurement of Particulate Flow in Discrete Structure Particle Heating Receivers," *ASME Paper No. ES2015-49510*.
- [23] Lee, T., Lim, S., Shin, S., Sadowski, D. L., Abdel-Khalik, S. I., Jeter, S. M., and Al-Ansary, H., 2015, "Numerical Simulation of Particulate Flow in Interconnected Porous Media for Central Particle-Heating Receiver Applications," *Sol. Energy*, **113**, pp. 14–24.
- [24] Ho, C. K., Christian, J. M., Romano, D., Yellowhair, J., Siegel, N., Savoldi, L., and Zanino, R., 2017, "Characterization of Particle Flow in a Free-Falling Solar Particle Receiver," *ASME J. Sol. Energy Eng.*, **139**(2), pp. 021011-1–032022-9.
- [25] Knott, R., Sadowski, D. L., Jeter, S. M., Abdel-Khalik, S. I., Al-Ansary, H. A., and El-Leathy, A., 2014, "High Temperature Durability of Solid Particles for Use in Particle Heating Concentrator Solar Power Systems," *ASME Paper No. ES2014-6586*.